Article

Not peer-reviewed version

Nonlocal Soft Plasmonics in Planar Homogeneous Multilayers

Preethi Ramesh Narayan and Christin David *

Posted Date: 4 August 2023

doi: 10.20944/preprints202308.0423.v1

Keywords: nanophotonics; spatial dispersion; nonlocality; theory and simulation

Article

Nonlocal Soft Plasmonics in Planar Homogeneous Multilayers

Preethi Ramesh Narayan [1,*] and Christin David [1,2,*]

[1] Institute of Condensed Matter Theory and Optics, Friedrich-Schiller-Universität Jena, Max-Wien-Platz 1, 07743 Jena, Germany
[2] Abbe Center of Photonics, Albert-Einstein-Straße 6, 07745 Jena, Germany
* Correspondence: christin.david@uni-jena.de

Abstract: Plasmonics is the study of resonant oscillations of free electrons in metals caused by incident electromagnetic radiation. Surface plasmons can focus and steer light on the subwavelength scale. Apart from metals, plasmonic phenomena can be observed in soft matter systems such as electrolytes where resonant charge oscillations can be induced for ions in solution. Due to their larger mass, they are plasmon-active in a lower frequency regime and on a larger wavelength scale. Spatial confinement allows increasingly strong charge interactions and gives rise to nonlocality or spatial dispersion effects. These effects manifest as additional longitudinal propagation modes and are known to cause plasmonic broadening and resonance shifts in metal nanostructures. We derive and discuss the nonlocal optical response of ionic plasmons using a hydrodynamic, two-fluid model in a planar homogeneous three-layer system with electrolyte-dielectric interfaces. Studying such systems enables us to identify and understand plasmonic phenomena in biological and chemical systems.

Keywords: nanophotonics; spatial dispersion; nonlocality; theory and simulation

1. Introduction

Free electrons in the conduction band of metals can be resonantly excited by incident light to form collective oscillations. If confined to a nanostructure in a dielectric environment, they form surface plasmons (SPs) manifesting along the conducting interface. At planar interfaces, surface plasmon polaritons (SPPs) are formed which propagate along the metal-dielectric interface with a higher parallel momentum compared to light in vacuum, while they decay exponentially away from the interface, as depicted in Figure 1(a). Consequently, they benefit from a long lifetime and enable the concentration of electromagnetic fields within dimensions approximately equal to or smaller than their wavelength [1]. This opens numerous possibilities for nanoscale applications including light generation and concentration through confinement effects [2,3], enhancement of nonlinear phenomena [4–8], optical data storage [9,10], improved solar cells [11–13] and photocatalysis [14], sensing down to the molecular level [15,16], surface-enhanced Raman spectroscopy [17,18], structure-induced colors [19,20], and much more.

Experimental observations show that short-ranged electron-electron interactions change the spectral profile of plasmons [21], which is contrary to the size-independence predicted by classical electrodynamics in the local response approximation (LRA). At length scales where the mean free path of valence electrons is similar to the particle diameter, quantum effects emerge leading to additional loss channels. Noble metal nanostructures [22–25], metallic dimers [23,26–29], and nanostructures with sub-nanometer gaps [30] exhibit significant blueshifts and quenching of their classically predicted near-field intensity.

To describe such effects, the hydrodynamic Drude model (HDM) is commonly integrated into standard computational nanophotonics methods. Spatial dispersion in metals has been described with Finite Element Method (FEM) [31], the analytical Wentzel-Kramers-Brillouin (WKB) method [31], time-dependent local density approximation (TDLDA) [27], Fourier Modal Method (FMM) [32], and

Preprints (www.preprints.org) | NOT PEER-REVIEWED | Posted: 4 August 2023 doi:10.20944/preprints202308.0423.v1

Transformation Optics (TO) [25]. To account for convection and electron diffusion, the HDM can be expanded into the generalized nonlocal optical response (GNOR) model [25,33–35].

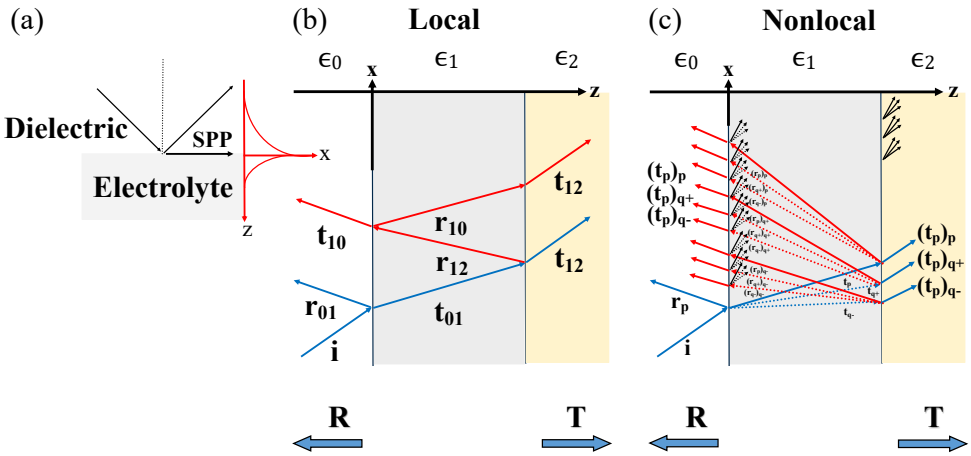

Figure 1. (**a**) Surface plasmon polariton (SPP) propagation at and its evanescent decay perpendicular to a dielectric-electrolyte interface. (**b**) In the local response approximation (LRA), a three-layer-system with dielectric constants ϵ_0, ϵ_1 and ϵ_2 shows the common multiple reflections for a single transversal mode. (**c**) With nonlocal optical response (NOR), multiple reflections of several modes of transversal and longitudinal character occur inside the electrolyte layer. Indices have been simplified.

Typically, plasmonics refers to the resonant excitation of the electron plasma. However, ionic charge carriers in soft matter such as membranes, biopolymers, liquid crystals, and complex fluids [36,37], also exhibit plasmonic behavior. These materials have a heterogeneous structure with sizes ranging from nanoscale to a few micrometers. Ions are much heavier than electrons, their concentration is much lower and their velocity depends on local temperature as we will detail out below. Consequently, different design principles and adapted analytical theories of plasmonics are needed to conceive soft matter systems that leverage plasmonic light-matter interactions. Ionic plasmon-polaritons have been investigated for spherical electrolytes, embedded e.g. in an insulating membrane, and chains thereof. Such models provide an alternative description of saltatory conduction observed in nerve cells [38]. In addition, loss mechanisms beyond classical electrodynamics such as size-dependent plasmon damping, ohmic-type energy dissipation, and radiative losses were discussed [39,40]. Nonlocal effects in soft plasmonics were investigated in spherical electrolyte systems using a two-fluid hydrodynamic model [40]. Such a two-fluid model was furthermore used to investigate nonlocal interaction in electron-hole pairs of semiconductors [41,42]. A generalized multi-fluid model has recently been developed [43].

In this article, we study the plasmonic properties of ions in solution in analogy to electrons in metals at planar homogeneous dielectric-electrolyte interfaces in systems depicted in Figs. 1(b) and 1(c), developing an analytic nonlocal two-fluid model that includes short-ranged non-classical interactions between the charge carriers resulting in spatial dispersion effects. Our study can provide insights into the underlying physics of ionic phenomena in biological and chemical systems, including energy transfer in nerve cells [44], and soft plasmons in photocatalysis.

2. Methodology

2.1. Classical soft plasmonics – General characteristics of ionic systems

Similarly to how electrons behave in metals, negative (-) ions in a fluid are displaced toward positive (+) ions and vice versa due to material polarization, leading to bulk plasma oscillations for each type of ion with frequency $\omega_{p_\pm}$

Preprints (www.preprints.org) | NOT PEER-REVIEWED | Posted: 4 August 2023 doi:10.20944/preprints202308.0423.v1

$$\omega_{p_\pm}^2 = \frac{Q_\pm^2 n_\pm}{\varepsilon_0 m_\pm} \tag{1}$$

which depends on their respective charge $Q_\pm$, mass $m_\pm$, and concentration $n_\pm$ [40]. Both positive and negative ions carry equal but opposite charge parities $Q_+ = -Q_-$ in our chosen materials. More generally, total charge balance is demanded, i.e. $|n_+ Q_+| = |n_- Q_-|$. Throughout this work, we set the ion concentration to $n_\pm = 1\text{mol/m}^3 N_A$, with the Avagadro constant N_A.

The ions are scattered throughout the entire electrolyte system and move in principle freely within the solution. The movement of ions within the electrolyte is influenced by their relatively large mass. Their mass is approximately 10^4 times greater than the mass of an electron, see Table 1. Ions exhibit a velocity determined by their sensitivity to thermal fluctuations, their thermal velocity $v_{th_\pm} = \sqrt{\frac{3k_B T}{m_\pm}}$, with values below 10^3 m/s at $T = 298.16$ K. Notably, ions of greater mass such as K^+ and Cl^- are slower than lighter ions like OH^- and H_3O^+. In contrast, free electrons in metals travel at a much higher speed, characterized by their Fermi velocity $v_F = \frac{\hbar k_F}{m_e}$, which is typically three to four orders of magnitude larger, e.g. for gold (and similarily for silver) $v_{F_{Au}} = 1.4 \times 10^6$ m/s [40]. Figure 2(a) shows that the values of ionic $\omega_{p_\pm}$ fall within the range of a few hundred GHz with heavier ions exhibiting decreasing $\omega_{p_\pm}$ values. Therefore, the plasmonic optical response of ionic systems occurs predominantly in the far-infrared.

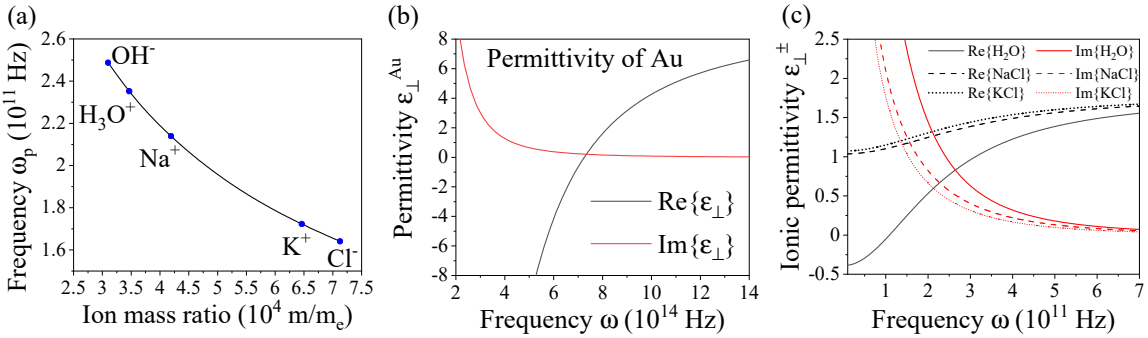

Figure 2. (**a**) Bulk plasmon frequency ω_p of OH^-, H_3O^+, Na^+, K^+, and Cl^- ions in solution varying with their respective ion mass ratios m/m_e with ion concentration $n_\pm = 1\text{mol/m}^3 N_A$, where N_A is the Avogadro constant. (**b**) Dielectric permittivity of Au in a simple Drude model varying with frequency using parameters $\omega_{p_{Au}} = 2.18 \times 10^{15}$ Hz, $\gamma_{Au} = 1.72 \times 10^{13}$ Hz, $\epsilon_{b_{Au}} = 9$ [45]. (**c**) Dielectric ionic permittivity of H_2O, NaCl, and KCl ions in solution varying with frequency with parameters as in Table 1 and background permittivity $\epsilon_b = 1.77$.

Table 1. Characteristic material parameters of ionic systems [40].

Ion	Mass ($\mathbf{m_e}$)	$\mathbf{m_\pm}$	Velocity $\mathbf{v_{th_\pm}}$ (m/s)	Frequency $\omega_{p_\pm}$ (10^{11} Hz)	Damping γ (10^{11} Hz)
OH^-	31005		663.63	2.49	2.46
H_3O^+	34670		627.57	2.35	2.20
Na^+	41907		570.82	2.14	3.19
K^+	64628		459.65	1.72	2.68
Cl^-	71270		437.71	1.64	3.07

When considering the contribution of both negative and positive ions to the optical response of an electrolyte, the dielectric Drude permittivity of ions can be employed as

Preprints (www.preprints.org) | NOT PEER-REVIEWED | Posted: 4 August 2023 doi:10.20944/preprints202308.0423.v1

$$\epsilon_{\perp}^{\pm}(\omega) = \epsilon_b - \frac{\omega_{p_+}^2}{\omega(\omega + i\gamma_+)} - \frac{\omega_{p_-}^2}{\omega(\omega + i\gamma_-)}. \tag{2}$$

Negative and positive ions operate with distinct plasmon bulk $\omega_{p_\pm}$ and damping frequencies $\gamma_\pm$ calculated from their viscosities, refer to Table 1 [40]. Figure 2(b) illustrates the characteristics of the dielectric function for Au in a Drude model enabling comparability with the behavior of ions in solution, Figure 2(c). Apart from operating in a distinct frequency range, ionic plasmons exhibit a typical plasmonic behavior similar to that of Au, that allows identifying the resonance condition at a planar interface $-\epsilon_0 = \mathrm{Re}\{\epsilon_{\perp}^{\pm}\}$. It should be noted that the dielectric permittivity ϵ_b is significantly lower for ions than that of noble metals such as Au ($\epsilon_{b,Au} \approx 10$) as it is determined by the solution in which the electrolytes move. Instead of a liquid, lipid matter with slightly higher $\epsilon_b \approx 2$ could be used. Neglecting damping, the resonance frequency ω_{SPP} at a planar metal interface is obtained from

$$\omega_{\mathrm{SPP}} = \frac{\omega_p}{\sqrt{2\epsilon_b}}, \tag{3}$$

which in the case of ions becomes

$$\omega_{\mathrm{SPP}_{ion}} = \sqrt{\frac{\omega_{p_+}^2 + \omega_{p_-}^2}{2\epsilon_b}}. \tag{4}$$

Finally, the dispersion relation of p-polarized SPPs that propagate at the interface separating two media as depicted in Figure 1(b) is given by

$$k_{\mathrm{SPP}} = \frac{\omega}{c}\sqrt{\frac{\epsilon_0\epsilon_1(\omega)}{\epsilon_0 + \epsilon_1(\omega)}}. \tag{5}$$

In Figure 3, we compare the analytical dispersion curve with the calculated energy flux in reflection of a Au-water interface, Figure 3(a), with ionized H_2O confined in neutral water to a slab of thickness $d = 2.5$ mm in Figure 3(b). The left side of the light line, the black line defined by $\omega = ck\epsilon_0$, represents propagating waves, while the right side corresponds to the excitation of bound SPPs. This excitation occurs for $k_{\parallel} > k_0$ [1]. Due to realistic damping in the system, propagating modes occur above the resonance frequency and bound modes show a finite width. While we observe the typical strong dispersion in Au due to the abundance of free electrons, the same signature is present in electrolytes with low concentration.

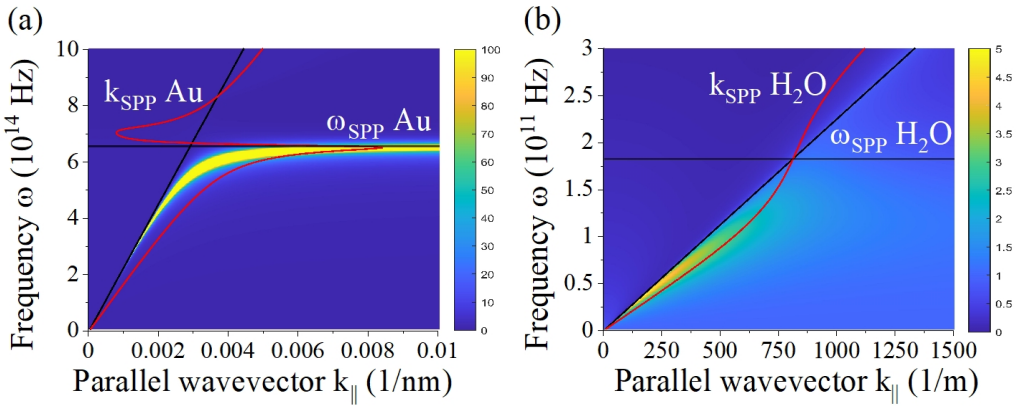

Figure 3. Analytical dispersion k_{SPP} (red curves) and reflected energy flux for (**a**) a Au-water interface and (**b**) ionized H_2O in a slab of thickness $d = 2.5$ mm. The position of ω_{SPP} (blue curves) and the light line (black curves) are marked for reference. Tabulated data was used for Au [45].

Preprints (www.preprints.org) | NOT PEER-REVIEWED | Posted: 4 August 2023 doi:10.20944/preprints202308.0423.v1

2.2. Nonlocal interactions in dielectric-electrolyte multilayered systems

Nonlocal phenomena occur when charge carriers interact over short length scales, typically promoted by strong spatial confinement [46]. This section focuses on nonlocal effects arising from ion-ion interactions driven by Coulombic forces in planar homogeneous multilayers. In order to study such systems, we apply the HDM to a two-fluid system [40]. In this framework, it was shown for ionic spheres that spatial dispersion yields less pronounced blueshifts of their plasmon resonances compared to metals [40].

The ion-ion interaction is described by the linearized Navier-Stokes equation

$$\mathbf{j}_{\pm} = \frac{i}{\omega + i\gamma_{\pm}}(\varepsilon_0 \omega_{p_{\pm}}^2 \mathbf{E} - \beta_{\pm}^2 \nabla \rho_{\pm}) \tag{6}$$

for an incident light field $\mathbf{E}$. The charges are treated separately in the usual wave equation as external current $j_{\pm}$ and charge densities $\rho_{\pm}$ arising from each charge carrier type. The nonlocal strength $\beta_{\pm} = \sqrt{\frac{3}{5}} v_{th_{\pm}}$ quantifies the interaction caused by internal pressure of the charge carriers. The Helmholtz equation for a nonlocal ionic system becomes

$$\nabla^2 \mathbf{E} + k^2 \epsilon_{\perp}^{\pm} \mathbf{E} = \frac{1}{\varepsilon_0} \nabla(\eta_- \rho_- + \eta_+ \rho_+), \tag{7}$$

where $\eta_{\pm} = \frac{1}{\epsilon_b} - \frac{k^2 \beta_{\pm}^2}{\omega(\omega + i\gamma_{\pm})}$ leading to a system of a total of three coupled equations.

An important manifestation of spatial dispersion is the emergence of longitudinal waves in addition to the usual transversal modes obtained by the Navier-Stokes equation as pressure waves of charge carriers. The classical transversal and additional longitudinal waves are superimposed in the nonlocal medium. The nonlocal wave vectors associated with the propagation of individual longitudinal ionic modes in a medium are

$$q_{\pm}^2 = \frac{1}{\beta_{\pm}^2} \frac{\omega(\omega + i\gamma_{\pm})}{\epsilon_b} \epsilon_{\perp_{\pm}}, \tag{8}$$

where $\epsilon_{\perp_{\pm}} = \epsilon_b - \frac{\omega_{p_{\pm}}^2}{\omega(\omega + i\gamma_{\pm})}$ is the individual permittivity of each type of ion which is not to be confused with the total ionic permittivity of the electrolyte given by $\epsilon_{\perp}^{\pm}$, see Equation (2).

The coupled nonlocal wave equations of each type of ion can be combined in to a single differential equation, symmetric with respect to the indicated signs, that results in a nonlocal wave equation of fourth order

$$0 = \beta_-^2 \beta_+^2 (\nabla^2 + q_-^2)(\nabla^2 + q_+^2)\rho_- - \frac{\omega_{p_+}^2 \omega_{p_-}^2}{\epsilon_b^2} \rho_-. \tag{9}$$

This gives rise to a fourth-power equation whose symmetric complex-valued roots describe the oscillations of positive and negative ions in an electrolyte system. Assuming a planar system and propagation in z-direction, the component of the wave vector of interest is q_z while the parallel component $\vec{k}_{\parallel}$ remains unchanged throughout the structure.

Figure 4(a) shows the resulting total nonlocal wave vector q_z as a function of the parallel wave vector $k_{\parallel}$ necessary to excite the longitudinal modes at planar interfaces. For the chosen frequency $\omega = 3 \times 10^{11}$ Hz, the values are in the range of $0.1 - 2$ nm^{-1}. Interestingly, a similar length scale is found for Au surfaces as depicted in Figure 4(b). The wave vector in propagation direction is connected to the penetration depth of the SPP waves that evanescently decay in the z-direction. The penetration or skin depth of nonlocal modes is given by $\delta = \frac{1}{Im\{q_z\}}$, which is of the order of 1 to 5 nm as depicted in Figure 4(c) for the ions.

Preprints (www.preprints.org) | NOT PEER-REVIEWED | Posted: 4 August 2023 doi:10.20944/preprints202308.0423.v1

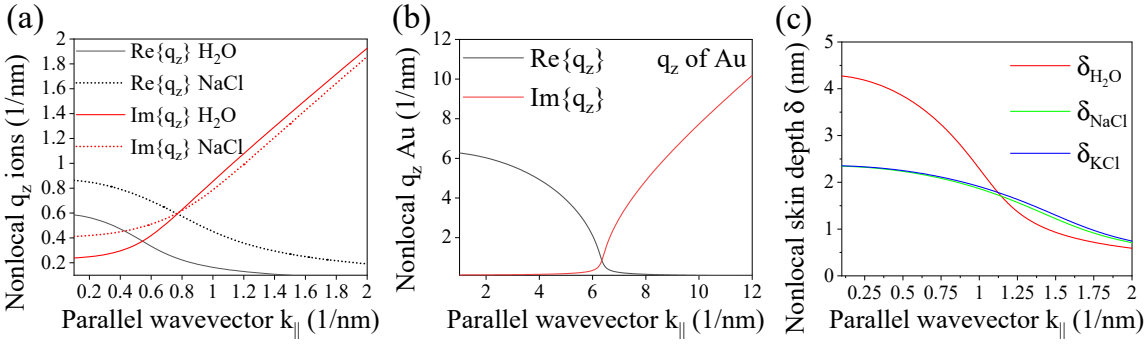

Figure 4. (**a**) Real and imaginary part of the nonlocal wave vector q_z of ions in solution varying with the parallel wave vector $k_\parallel$ for frequency $\omega = 3 \times 10^{11}$ Hz. (**b**) Same for Au at frequency $\omega = 10^{15}$ Hz. (**c**) Nonlocal skin depth $\delta = \frac{1}{Im\{q_z\}}$ of ions in solution.

3. Results and Discussion

3.1. Nonlocal optical coefficients for finite multilayers

In this section, we derive the optical coefficients at planar dielectric-electrolyte interfaces with either transversal or longitudinal incident modes as illustrated in Figure 1(c). The usual boundary conditions, i.e. the continuity of the parallel field components of the electric and magnetic fields, are applied next to an additional boundary condition (ABC) emerging from the hydrodynamic model for each type of ion. In a hard-wall boundary approach, it is given by $\hat{n} \cdot \mathbf{j}_\pm = 0$, where $\hat{n}$ is the surface normal, and determines the amplitude of longitudinal waves. Due to the overall micrometer size of ionic systems and larger mass of individual ions than compared to electrons, further surface effects are negligible [40,47,48].

The system is, thus, described by a total of three possible modes, the transversal p and longitudinal $q_\pm$ excitations, through their wave vectors in z-direction $k_{z_1} = \sqrt{(\frac{\omega}{c})^2 \epsilon_\perp^\pm - k_\parallel^2}$ and q_z given by the roots of the fourth-power equation (9) discussed above.

In general, several distinct cases are possible. Within the dielectric, only the transversal mode (p) can be excited. At a dielectric-electrolyte interface, i.e. light incident from the dielectric side and propagation in $+z$-direction, the light transmitted into the electrolyte medium excites a transversal and both longitudinal modes $q_\pm$ according to their respective transmission coefficients. On the other hand, in reflection only the transversal mode (p) remains. For an electrolyte-dielectric interface, any of the three modes may be incident on the interface and likewise reflected back into the electrolyte, but again, in transmission only the transversal mode will be excited.

Let us consider as an examplary case light incident from the dielectric side, characterized by permititvity ϵ_0. It is partially reflected back into the dielectric medium as r_{01p} and the remainder is transmitted into the electrolyte medium of permittivity $\epsilon_1 = \epsilon_\perp^\pm$ and divided into three modes, namely the transversal mode t_{01p}, and the longitudinal modes $t_{01q\pm}$. Solving the three boundary conditions mentioned above leads to the nonlocal Fresnel coefficients for a two-fluid system

$$r_{01p} = \frac{(1+g'_{soft})\epsilon_\perp^\pm k_{z_0} - (1+g_{soft})\epsilon_0 k_{z_1}}{(1+g'_{soft})\epsilon_\perp^\pm k_{z_0} + (1+g_{soft})\epsilon_0 k_{z_1}}, \quad t_{01p} = \frac{2k_{z_0}\frac{k_1}{k_0}\epsilon_0}{(1+g'_{soft})\epsilon_\perp^\pm k_{z_0} + (1+g_{soft})\epsilon_0 k_{z_1}}$$

where g_{soft} and g'_{soft} stem from the nonlocal properties with

$$g_{soft} = \frac{k_\parallel k_1}{k_{z_1}} \left(\frac{F_{l_+}}{|q_+|} + \frac{F_{l_-}}{|q_-|} \right), \tag{10}$$

$$g'_{soft} = \frac{-ik_1 q_z}{k_\parallel} \left(\frac{F_{l_+}}{|q_+|} + \frac{F_{l_-}}{|q_-|} \right). \tag{11}$$

Preprints (www.preprints.org) | NOT PEER-REVIEWED | Posted: 4 August 2023 doi:10.20944/preprints202308.0423.v1

Finally, the ABC connects the longitudinal modes with the transversal mode via

$$t_{01q_\pm} = F_{l_\pm} t_{01p}. \tag{12}$$

In the (local) limit $k_\parallel \to 0$, the common Fresnel coefficients of the LRA can be retrieved, i.e. for planar systems all coefficients become local at normal incidence as at least some parallel momentum is needed to excite the longitudinal modes. Further details, e.g. on the additional nonlocal function $F_{l_\pm}$ can be found in the Appendix.

For a three-layered system, e.g. an electrolyte layer of finite width d in neutral solution as depicted in Figure 1(c), a high complexity of involved modes emerges due to the multiple reflection events as each interaction with an interface creates three further excitations.

Let us consider the total transmission coefficient T. The part of the incident light that transmits into the electrolyte medium splits into three modes with amplitudes t_{01p}, t_{01q+}, and t_{01q-}. When reaching the second interface, these modes can transmit into the second dielectric medium with amplitude t_{12p} or be reflected back as r_{12p}, r_{12q+}, and r_{12q-}. A second index is necessary to indicate both, the original mode and the type of mode that was excited by it as the respective optical coefficients differ from each other. Further internal reflections occur and all triple possibilities with the respective double index are $[(r_{10p})_p, (r_{10q+})_p, (r_{10q-})_p]$, $[(r_{10p})_{q+}, (r_{10q+})_{q+}, (r_{10q-})_{q+}]$, and $[(r_{10p})_{q-}, (r_{10q+})_{q-}, (r_{10q-})_{q-}]$. For transmission, all contributions exiting the second interface towards the outer medium are summed up. Depending on the nature of the wave incident to the interface, the related coefficients are $[(t_{12p})_p, (t_{12p})_{q+}$, and $(t_{12p})_{q-}]$. The described optical paths are the typical multiple reflections observed in a Fabry-Pérot setup, however, each interaction with an interface creates three modes inside the nonlocal electrolyte. This allows writing the total reflection and transmission coefficients in the known manner. All related electric fields are superimposed and contribute to the total transmission coefficient T

$$T = \frac{(\mathrm{I})_T (\mathrm{III})_T}{1 - (\mathrm{II})_T}, \tag{13}$$

where $(\mathrm{I})_T$ and $(\mathrm{III})_T$ are the transmission contributions from the three excitations

$$(\mathrm{I})_T = t_{01p} e^{ik_{z_1} d} + t_{01q+} e^{iq_z d} + t_{01q-} e^{iq_z d}, \qquad (\mathrm{III})_T = (t_{12p})_p + (t_{12q+})_{q+} + (t_{12q-})_{q-}.$$

They describe the initial transmission step into the electrolyte layer and the final transmission step into the outer dielectric layer, respectively. The term $(\mathrm{II})_T$ describes the multiple internal reflections. Here, all possible modes are excited and this contribution becomes rather involved. The analytic expression can be found in the Appendix.

The total reflection coefficient R can be derived in a similar manner and can be cast into the standard form for a three-layer system

$$R = r_{01p} + \frac{(\mathrm{I})_R (\mathrm{II})_R (\mathrm{III})_R}{1 - (\mathrm{II})_T}, \tag{14}$$

where the coefficient describing the inner multiple reflections, $(\mathrm{II})_T$, is unchanged. The term $(\mathrm{II})_R$ describes the reflection at the second interface and can be found in the Appendix. $(\mathrm{I})_R$ and $(\mathrm{III})_R$ contain the initial transmission into the electrolyte layer and the final transmission back into the front layer. They are given by

$$(\mathrm{I})_R = t_{01p} e^{ik_{z_1} d} + t_{01q+} e^{iq_z d} + t_{01q-} e^{iq_z d}, \qquad (\mathrm{III})_R = (t_{10p})_p + (t_{10p})_{q+} + (t_{10p})_{q-}.$$

It is notable that from analyzing the optical paths of all modes both the total transmission and reflection for the case of nonlocal interaction between ions can be cast into the familiar form known from classical electrodynamics. While the contributions are given by summations of transversal and longitudinal

Preprints (www.preprints.org) | NOT PEER-REVIEWED | Posted: 4 August 2023 doi:10.20944/preprints202308.0423.v1

solutions, this analysis allows systematically increasing the complexity to multi-fluid systems with more distinct constituents.

3.2. Evaluating three-layer systems

In an experimental setup, reflection and transmission are measured in terms of energy flux retrieved from the time-averaged real part of the Poynting vector $\mathbf{S} = \mathbf{E} \times \mathbf{H}^*$. The flux of light incident in the dielectric is $\langle \mathbf{S}_0 \rangle = \frac{1}{2}\varepsilon_0 \frac{c^2}{\omega} Re\{k_0\} |\mathbf{E}_0|^2$, and changes for reflected light to $\langle \mathbf{S}_r \rangle = \frac{1}{2}\varepsilon_0 \frac{c^2}{\omega} Re\{k_r\} |\mathbf{E}_r|^2$, and results for transmitted light in $\langle \mathbf{S}_t \rangle = \frac{1}{2}\varepsilon_0 \frac{c^2}{\omega} Re\{k_t\} |\mathbf{E}_t|^2$, where $k_r = k_0$. From this, we calculate the reflected and transmitted energy flux

$$R_{flux} = \frac{|\langle \mathbf{S}_r \rangle|}{|\langle \mathbf{S}_0 \rangle|} = |R|^2 \frac{Re\{k_r\}}{Re\{k_0\}}, \qquad T_{flux} = \frac{|\langle \mathbf{S}_t \rangle|}{|\langle \mathbf{S}_0 \rangle|} = |T|^2 \frac{Re\{k_t\}}{Re\{k_0\}}. \tag{15}$$

The wave vectors in the dielectric media are $k_0 = \sqrt{(\frac{\omega}{c})^2 \epsilon_0 - k_\parallel^2}$ and $k_t = \sqrt{(\frac{\omega}{c})^2 \epsilon_2 - k_\parallel^2}$. Note that the flux can be greater than 1 in the evanescent regime at high parallel momenta, however, the flux of the associated evanescent waves does not carry energy.

We compare spectra of the fluxes for a nonlocal system in a water-electrolyte-water configuration with its local case in Figure 5 using the material parameters given in Table 1 for the different ionic systems. Firstly, we consider in Figure 5(a) a nonlocal electrolyte layer with thickness $d = 1$ mm at a fixed parallel momentum. We observe a considerable amount of plasmonic resonance broadening for the T_{flux} in the upper and R_{flux} in the lower panel as compared to the sharp resonances in the local case in Figure 5(b), in particular for the resonant reflection. The broadening is stronger for lighter ions. This is due to the nonlocal strength parameter β being larger for faster ions, which is the case for the lighter ions, since the thermal velocity is inversely proportional to their mass.

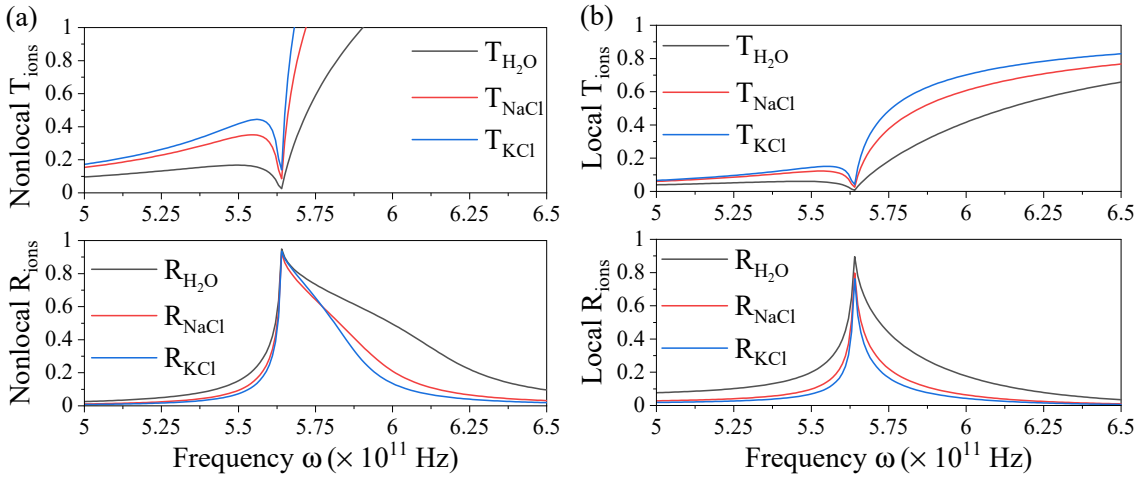

Figure 5. Transmission (upper panel) and reflection spectra (lower panel) of ions in solution in the (**a**) nonlocal and (**b**) local case for an electrolyte layer of thickness $d = 1$ mm and with parallel momentum $k_\parallel = 2500\ \mathrm{m}^{-1}$.

The flux can become larger than 1 in the evanescent regime where $k_0 < k_\parallel$. The transition into this regime occurs past the resonance frequency and explains the increase observed in T. The associated modes are evanescent and do not carry information at this large parallel momentum. For reasonably low parallel momentum, the measurable transmission converges to the local result. Hence, the measured transmission will reach close to 100% in this regime which can still be assessed from $1 - R_{flux}$. The absorption reaching zero can additionally be seen in Figure 2(c).

We compare spectra of the fluxes for a nonlocal system in a water-electrolyte-water configuration with its local case in Figure 6 varying the thickness of the electrolyte layer. The highest T is observed for

Preprints (www.preprints.org) | NOT PEER-REVIEWED | Posted: 4 August 2023 doi:10.20944/preprints202308.0423.v1

the lowest thickness and vice-versa for reflection which can be expected for the only slightly absorbing material. The reflection peaks become broader for lower layer thickness where the nonlocal strength increases. The resonance position is stable, any induced blue shift as observed in solid metal nonlocal systems [21,23,24,26,31,34] is not resolved in this frequency regime. In metal systems, such a shift results in a few tens of nanometers for highly nonlocal systems. In ionic systems, where the resonance wavelength is several orders of magnitude larger, such a shift does not have an impact given the broadening of the peaks with increased nonlocal interaction. As before, the transmitted flux becomes larger than 1 in the evanescent regime past the resonance frequency, but reduces to the local result when decreasing the parallel momentum.

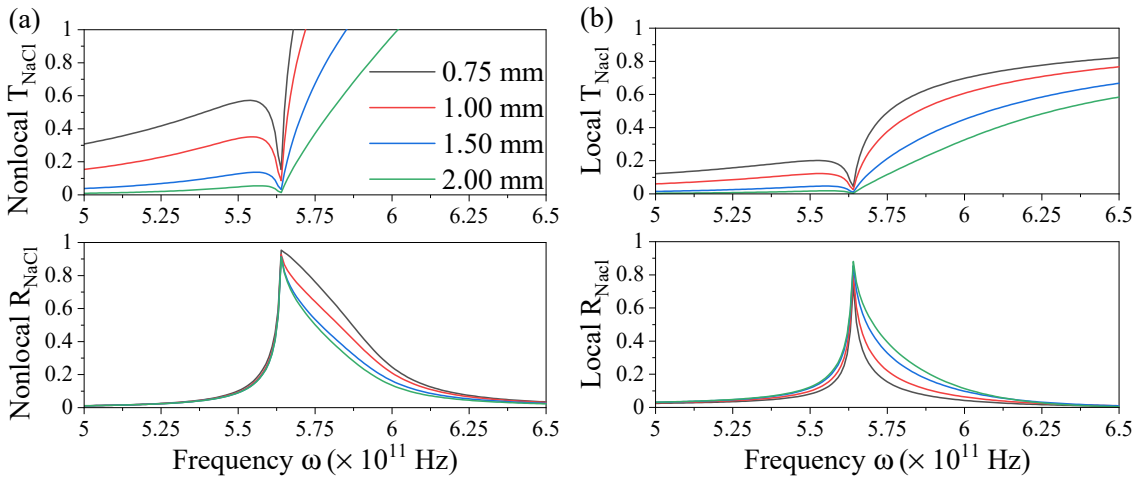

Figure 6. Transmission (upper panel) and reflection spectra (lower panel) of ionized NaCl in solution in the (**a**) nonlocal and (**b**) local case for varying layer thickness $d = 1$ mm and with parallel momentum $k_{||} = 2500\ \mathrm{m}^{-1}$.

4. Conclusions

We studied the nonlocal plasmonic response of planar electrolyte-dielectric interfaces in comparison to the local response approximation of classical electrodynamics. We believe that there is a need to create an understanding of plasmonics beyond electrons in solid matter. Ions are resonant in the far-infrared and are typically confined to mesoscopic length scales in the range of a few hundred microns, e.g. in biological systems. Their analytical plasmonic dispersion curve exhibits weak SPPs due to typically low charge carrier concentration. These fundamental properties arise due to their large mass $\sim 10^4 m_e$ resulting in low thermal velocities $v_{th_\pm}$ which determines the interaction strengths of nonlocal charge carrier interaction. Overall, their plasmonic behavior is comparable to electrons in metals. However, they offer a wider range of tunability by choice of material allowing to adjust material mass, charge and concentration.

In addition to studying classical plasmonic properties of ions in a planar electrolyte layer, we use the hydrodynamic, two-fluid model to assess spatial dispersion effects in ionic systems. A coupled dynamics of the negative and positive ions is obtained from the analytical expressions of charge densities. In a three-layered system with dielectric-electrolyte interfaces, the complexity is increased by the additional longitudinal modes associated with nonlocal wave numbers $q_\pm$. This manifests as resonance broadening of the energy flux. The wave amplitudes of these modes were obtained from the additional boundary condition at the electrolyte-dielectric interfaces. In the $k_{||} \to 0$ limit of the nonlocal analytical expressions, we retrieve the original expressions for the local response.

We conclude from these results that a notable difference in the optical coefficients arises in ionic fluids confined to a planar slab when ion-ion interaction is considered. Our analysis allows increasing systematically the complexity further to a three-layered multi-fluid ionic system, where the contributions stem from more than two ionic constituents. Exploiting the plasmonic properties of ions

Preprints (www.preprints.org) | NOT PEER-REVIEWED | Posted: 4 August 2023 doi:10.20944/preprints202308.0423.v1

can open up new avenues in their description and, thus, understanding of their behaviour. We believe that extending plasmonics towards soft matter can bridge soft and hard matter regimes with potential applications in biology and chemistry.

Author Contributions: Conceptualization, C.D.; methodology, C.D.; software, P.R.N.; validation, P.R.N. and C.D.; formal analysis, P.R.N.; writing—original draft preparation, P.R.N.; writing—review and editing, P.R.N. and C.D.; visualization, P.R.N.; funding acquisition, C.D.

Funding: We acknowledge financial support by the program *ProChance*^{career} of the Friedrich-Schiller-University Jena (2.11.3-A1/2020-02). This article is the result of P.R.N.'s research project within the framework of the *Honours Program for Future Researchers* at the Friedrich Schiller University Jena, Germany, funded by the Excellence Strategy of the German State Government and the Länder. The APC was kindly waived for this invited contribution.

Institutional Review Board Statement: Not applicable.

Informed Consent Statement: Not applicable.

Data Availability Statement: The datasets generated and analyzed during the presented study are available upon reasonable request from the corresponding author.

Conflicts of Interest: The authors declare no conflict of interest.

Appendix A. Nonlocal function $F_{l_\pm}$

The function $F_{l_\pm}$ connects the optical coefficients of the longitudinal with the transversal modes Equation (12) and is found after applying the respective boundary conditions and solving the resulting system of linear equations. Its analytic expression is

$$F_{l_\pm} = \frac{\omega_{p_\pm}^2 \varepsilon_0 |q_z|(1+\beta'_\mp)}{i q_z \kappa_\pm (1-\alpha')} \left(\frac{-k_\parallel}{k}\right). \tag{A1}$$

where $\kappa_\pm$, α', and $\beta'_\mp$ are given by

$$\kappa_\pm = \beta_\pm^2 - \frac{\omega_{p_\pm}^2 \varepsilon_0}{k^2\epsilon_\perp^\pm - (k_\parallel^2 + q_z^2)} \left(\frac{1}{\epsilon_b} - \frac{k^2\beta_\mp^2}{\omega(\omega + i\gamma_\mp)}\right) \tag{A2}$$

$$\alpha' = \frac{\omega_{p_+}^2 \omega_{p_-}^2 \varepsilon_0^2}{\kappa_+\kappa_-(k^2\epsilon_\perp^\pm - (k_\parallel^2 + q_z^2))^2} \left(\frac{1}{\epsilon_b} - \frac{k^2\beta_+^2}{\omega(\omega + i\gamma_+)}\right)\left(\frac{1}{\epsilon_b} - \frac{k^2\beta_-^2}{\omega(\omega + i\gamma_-)}\right) \tag{A3}$$

$$\beta'_\mp = \frac{\omega_{p_\pm}^2 \varepsilon_0}{\kappa_\pm(k^2\epsilon_\perp^\pm - (k_\parallel^2 + q_z^2))} \left(\frac{1}{\epsilon_b} - \frac{k^2\beta_\mp^2}{\omega(\omega + i\gamma_\mp)}\right). \tag{A4}$$

Appendix B. Nonlocal transmission and reflection coefficients

The terms that contribute to $(\mathrm{II})_T$ to the total transmission coefficient T, eq. (13), are

$$\begin{aligned}(\mathrm{II})_T = {} & \{(r_{10p})_p + (r_{10q+})_p + (r_{10q-})_p\} e^{ik_{z_1}d} \{(r_{12p})_p e^{ik_{z_1}d} + (r_{12q+})_{q+} e^{iq_z d} + (r_{12q-})_{q-} e^{iq_z d}\} \\ & + \{(r_{10p})_{q+} + (r_{10q+})_{q+} + (r_{10q-})_{q+}\} e^{iq_z d} \{(r_{12q+})_p e^{ik_{z_1}d} + (r_{12q+})_{q+} e^{iq_z d} + (r_{12q+})_{q-} e^{iq_z d}\} \\ & + \{(r_{10p})_{q-} + (r_{10q+})_{q-} + (r_{10q-})_{q-}\} e^{iq_z d} \{(r_{12q-})_p e^{ik_{z_1}d} + (r_{12q-})_{q+} e^{iq_z d} + (r_{12q-})_{q-} e^{iq_z d}\}.\end{aligned}$$

In the total reflection coefficient R, eq. (14), the following terms contribute to $(\mathrm{II})_R$.

$$\begin{aligned}(\mathrm{II})_R = {} & \{(r_{12p})_p + (r_{12q+})_p + (r_{12q-})_p\} e^{ik_{z_1}d} + \{(r_{12p})_{q+} + (r_{12q+})_{q+} + (r_{12q-})_{q+}\} e^{iq_z d} \\ & + \{(r_{12p})_{q-} + (r_{12q+})_{q-} + (r_{12q-})_{q-}\} e^{iq_z d}.\end{aligned}$$

References

1. Maier, S.A. *Plasmonics: Fundamentals and Applications*; Springer US, 2007. doi:10.1007/0-387-37825-1.
2. Schuller, J.A.; Barnard, E.S.; Cai, W.; Jun, Y.C.; White, J.S.; Brongersma, M.L. Plasmonics for extreme light concentration and manipulation. *Nat. Mater.* **2010**, *9*, 193–204.
3. Luo, Y.; Chamanzar, M.; Adibi, A. Compact on-chip plasmonic light concentration based on a hybrid photonic-plasmonic structure. *Optics Express* **2013**, *21*, 1898. doi:10.1364/oe.21.001898.
4. Kauranen, M.; Zayats, A.V. Nonlinear plasmonics. *Nature Photonics* **2012**, *6*, 737–748. doi:10.1038/nphoton.2012.244.
5. Krasavin Alexey, V.; Pavel, G.; Zayats Anatoly, V. Free-electron Optical Nonlinearities in Plasmonic Nanostructures: A Review of the Hydrodynamic Description. *Laser & Photonics Reviews* **2018**, *12*, 1700082. doi:10.1002/lpor.201700082.
6. Mesch, M.; Metzger, B.; Hentschel, M.; Giessen, H. Nonlinear Plasmonic Sensing. *Nano Letters* **2016**, *16*, 3155–3159. doi:10.1021/acs.nanolett.6b00478.
7. Beer, S.; Gour, J.; Alberucci, A.; David, C.; Nolte, S.; Zeitner, U.D. Second harmonic generation under doubly resonant lattice plasmon excitation. *Optics Express* **2022**, *30*, 40884. doi:10.1364/oe.470578.
8. Daryakar, N.; David, C. Thin Films of Nonlinear Metallic Amorphous Composites. *Nanomaterials* **2022**, *12*, 3359. doi:10.3390/nano12193359.
9. Zhang, C.; Ji, M.; Zhou, X.; Mi, X.; Chen, H.; Zhang, B.; Fu, Z.; Zhang, Z.; Zheng, H. Plasmon-Assisted Self-Encrypted All-Optical Memory. *Advanced Functional Materials* **2022**, *33*, 2208561. doi:10.1002/adfm.202208561.
10. Taylor, A.B.; Michaux, P.; Mohsin, A.S.M.; Chon, J.W.M. Electron-beam lithography of plasmonic nanorod arrays for multilayered optical storage. *Optics Express* **2014**, *22*, 13234. doi:10.1364/oe.22.013234.
11. Green, M.A.; Pillai, S. Harnessing plasmonics for solar cells. *Nat Photon* **2012**, *6*, 130–132.
12. Enrichi, F.; Quandt, A.; Righini, G. Plasmonic enhanced solar cells: Summary of possible strategies and recent results. *Renewable and Sustainable Energy Reviews* **2018**, *82*, 2433–2439. doi:10.1016/j.rser.2017.08.094.
13. David, C.; Koduvelikulathu, L.J.; Kopecek, R. Comparative Simulations of Conductive Nitrides as Alternative Plasmonic Nanostructures for Solar Cells. *14*, 4236. doi:10.3390/en14144236.
14. Fusco, Z.; Catchpole, K.; Beck, F.J. Investigation of the mechanisms of plasmon-mediated photocatalysis: synergistic contribution of near-field and charge transfer effects. *Journal of Materials Chemistry C* **2022**, *10*, 7511–7524. doi:10.1039/d2tc00491g.
15. Taylor, A.B.; Zijlstra, P. Single-Molecule Plasmon Sensing: Current Status and Future Prospects. *ACS Sensors* **2017**, *2*, 1103–1122. doi:10.1021/acssensors.7b00382.
16. Zhou, X.L.; Yang, Y.; Wang, S.; Liu, X.W. Surface Plasmon Resonance Microscopy: From Single-Molecule Sensing to Single-Cell Imaging. *Angewandte Chemie International Edition* **2020**, *59*, 1776–1785. doi:10.1002/anie.201908806.
17. Sharma, B.; Frontiera, R.R.; Henry, A.I.; Ringe, E.; Duyne, R.P.V. SERS: Materials, applications, and the future. *Materials Today* **2012**, *15*, 16–25. doi:10.1016/s1369-7021(12)70017-2.
18. Schlücker, S. Surface-Enhanced Raman Spectroscopy: Concepts and Chemical Applications. *Angewandte Chemie International Edition* **2014**, *53*, 4756–4795. doi:10.1002/anie.201205748.
19. Stockman, M.I.; Kneipp, K.; Bozhevolnyi, S.I.; Saha, S.; Dutta, A.; Ndukaife, J.; Kinsey, N.; Reddy, H.; Guler, U.; Shalaev, V.M.; Boltasseva, A.; Gholipour, B.; Krishnamoorthy, H.N.S.; MacDonald, K.F.; Soci, C.; Zheludev, N.I.; Savinov, V.; Singh, R.; Groß, P.; Lienau, C.; Vadai, M.; Solomon, M.L.; Barton, D.R.; Lawrence, M.; Dionne, J.A.; Boriskina, S.V.; Esteban, R.; Aizpurua, J.; Zhang, X.; Yang, S.; Wang, D.; Wang, W.; Odom, T.W.; Accanto, N.; de Roque, P.M.; Hancu, I.M.; Piatkowski, L.; van Hulst, N.F.; Kling, M.F. Roadmap on plasmonics. *Journal of Optics* **2018**, *20*, 043001. doi:10.1088/2040-8986/aaa114.
20. Rezaei, S.D.; Dong, Z.; Chan, J.Y.E.; Trisno, J.; Ng, R.J.H.; Ruan, Q.; Qiu, C.W.; Mortensen, N.A.; Yang, J.K. Nanophotonic Structural Colors. *ACS Photonics* **2020**, *8*, 18–33. doi:10.1021/acsphotonics.0c00947.
21. García de Abajo, F.J. Nonlocal Effects in the Plasmons of Strongly Interacting Nanoparticles, Dimers, and Waveguides. *J. Phys. Chem. C* **2008**, *112*, 17983–17987.
22. Scholl, J.A.; Koh, A.L.; Dionne, J.A. Quantum plasmon resonances of individual metallic nanoparticles. *Nature* **2012**, *483*, 421–427.

23. David, C.; García de Abajo, F.J. Spatial Nonlocality in the Optical Response of Metal Nanoparticles. *J. Phys. Chem. C* **2011**, *115*, 19470–19475.
24. Raza, S.; Stenger, N.; Kadkhodazadeh, S.; Fischer, S.V.; Kostesha, N.; Jauho, A.P.; Burrows, A.; Wubs, M.; Mortensen, N.A. Blueshift of the surface plasmon resonance in silver nanoparticles studied with EELS. *Nanophotonics* **2013**, *2*, 131.
25. Raza, S.; Bozhevolnyi, S.I.; Wubs, M.; Mortensen, N.A. Nonlocal optical response in metallic nanostructures. *J. Phys. Cond. Matter.* **2015**, *27*, 183204.
26. Fernández-Domínguez, A.I.; Wiener, A.; García-Vidal, F.J.; Maier, S.A.; Pendry, J.B. Transformation-Optics Description of Nonlocal Effects in Plasmonic Nanostructures. *Phys. Rev. Lett.* **2012**, *108*, 106802.
27. Zuloaga, J.; Prodan, E.; Nordlander, P. Quantum Description of the Plasmon Resonances of a Nanoparticle Dimer. *Nano Lett.* **2009**, *9*, 887–891.
28. Ciracì, C.; Hill, R.T.; Mock, J.J.; Urzhumov, Y.; Fernández-Domínguez, A.I.; Maier, S.A.; Pendry, J.B.; Chilkoti, A.; Smith, D.R. Probing the Ultimate Limits of Plasmonic Enhancement. *Science* **2012**, *337*, 1072–1074.
29. Toscano, G.; Straubel, J.; Kwiatkowski, A.; Rockstuhl, C.; Evers, F.; Xu, H.; Mortensen, N.A.; Wubs, M. Resonance shifts and spill-out effects in self-consistent hydrodynamic nanoplasmonics. *Nat. Commun.* **2015**, *6*, 7132. doi:10.1038/ncomms8132.
30. Zhu, W.; Esteban, R.; Borisov, A.G.; Baumberg, J.J.; Nordlander, P.; Lezec, H.J.; Aizpurua, J.; Crozier, K.B. Quantum mechanical effects in plasmonic structures with subnanometre gaps. *Nature Communications* **2016**, *7*. doi:10.1038/ncomms11495.
31. Wiener, A.; Fernández-Domínguez, A.I.; Horsfield, A.P.; Pendry, J.B.; Maier, S.A. Nonlocal Effects in the Nanofocusing Performance of Plasmonic Tips. *Nano Lett.* **2012**, *12*, 3308–3314.
32. David, C.; Christensen, J.; Mortensen, N.A. Spatial dispersion in two-dimensional plasmonic crystals: Large blueshifts promoted by diffraction anomalies. *Phys. Rev. B* **2016**, *94*, 165410.
33. Mortensen, N.A.; Raza, S.; Wubs, M.; Søndergaard, T.; Bozhevolnyi, S.I. A generalized non-local optical response theory for plasmonic nanostructures. *Nat. Commun.* **2014**, *5*, 3809.
34. Raza, S.; Wubs, M.; Bozhevolnyi, S.I.; Mortensen, N.A. Nonlocal study of ultimate plasmon hybridization. *Opt. Lett.* **2015**, *40*, 839–842.
35. Mortensen, N.A. Mesoscopic electrodynamics at metal surfaces. *Nanophotonics* **2021**, *10*, 2563–2616. doi:10.1515/nanoph-2021-0156.
36. Kolle, M.; Lee, S. Progress and Opportunities in Soft Photonics and Biologically Inspired Optics. *Advanced Materials* **2017**, *30*, 1702669. doi:10.1002/adma.201702669.
37. van der Gucht, J. Grand Challenges in Soft Matter Physics. *Frontiers in Physics* **2018**, *6*. doi:10.3389/fphy.2018.00087.
38. Jacak, J.; Jacak, W. Plasmons and Plasmon–Polaritons in Finite Ionic Systems: Toward Soft-Plasmonics of Confined Electrolyte Structures. *Applied Sciences* **2019**, *9*, 1159. doi:10.3390/app9061159.
39. Jacak, W.A. Plasmons in finite spherical electrolyte systems: RPA effective jellium model for ionic plasma excitations. *Plasmonics* **2016**, *11*, 637–651. doi:10.1007/s11468-015-0064-6.
40. David, C. Two-fluid, hydrodynamic model for spherical electrolyte systems. *Scientific Reports* **2018**, *8*, 7544. doi:10.1038/s41598-018-25791-0.
41. Maack, J.R.; Mortensen, N.A.; Wubs, M. Size-dependent nonlocal effects in plasmonic semiconductor particles. *EPL (Europhysics Letters)* **2017**, *119*, 17003. doi:10.1209/0295-5075/119/17003.
42. Maack, J.R.; Mortensen, N.A.; Wubs, M. Two-fluid hydrodynamic model for semiconductors. *Physical Review B* **2018**, *97*. doi:10.1103/physrevb.97.115415.
43. Dong, T.; Yin, K.; Gao, X.; Ma, X. Generalized local analogue model for nonlocal plasmonic nanostructures based on multiple-fluid hydrodynamic framework. *Journal of Physics D: Applied Physics* **2020**, *53*, 295105. doi:10.1088/1361-6463/ab8509.
44. Jacak, J.E.; Jacak, W.A. New wave-type mechanism of saltatory conduction in myelinated axons and micro-saltatory conduction in C fibres. *European Biophysics Journal* **2020**, *49*, 343–360. doi:10.1007/s00249-020-01442-z.
45. Johnson, P.B.; Christy, R.W. Optical Constants of noble metals. *Phys. Rev. B* **1972**, *6*, 4370–4379.
46. Kluczyk, K.; Jacak, L.; Jacak, W.; David, C. Microscopic Electron Dynamics in Metal Nanoparticles for Photovoltaic Systems. *Materials* **2018**, *11*, 1077. doi:10.3390/ma11071077.

47. Toscano, G.; Raza, S.; Jauho, A.P.; Mortensen, N.A.; Wubs, M. Modified field enhancement and extinction by plasmonic nanowire dimers due to nonlocal response. *Opt. Express* **2012**, *20*, 4176–4188.
48. David, C.; García de Abajo, F.J. Surface Plasmon Dependence on the Electron Density Profile at Metal Surfaces. *ACS Nano* **2014**, *8*, 9558–9566. doi:10.1021/nn5038527.